JACS
JOURNAL OF THE AMERICAN CHEMICAL SOCIETY

Article

pubs.acs.org/JACS

Crystal Fluidity Reflected by Fast Rotational Motion at the Core, Branches, and Peripheral Aromatic Groups of a Dendrimeric Molecular Rotor

Xing Jiang, Zachary J. O'Brien, Song Yang, Lan Huong Lai, Jeffrey Buenaflor, Colleen Tan, Saeed Khan, K. N. Houk,* and Miguel A. Garcia-Garibay*

Department of Chemistry and Biochemistry, University of California, Los Angeles, California 90095-1569, United States

Supporting Information

ABSTRACT: Low packing densities are key structural features of amphidynamic crystals built with static and mobile components. Here we report a loosely packed crystal of dendrimeric rotor **2** and the fast dynamics of all its aromatic groups, both resulting from the hyperbranched structure of the molecule. Compound **2** was synthesized with a convergent strategy to construct a central phenylene core with stators consisting of two layers of triarylmethyl groups. Single crystal X-ray diffraction analysis confirmed a low-density packing structure consisting of one molecule of **2** and approximately eight solvent molecules per unit cell. Three isotopologues of **2** were synthesized to study the motion of each segment of the molecule in the solid state using variable temperature quadrupolar echo ^{2}H NMR spectroscopy. Line shape analysis of the spectra reveals that the central phenylene, the six branch phenylenes, and the 18 periphery phenyls all display megahertz rotational dynamics in the crystals at ambient temperature. Arrhenius analysis of the data gives similar activation energies and pre-exponential factors for different parts of the structure. The observed pre-exponential factors are 4−6 orders of magnitude greater than those of elementary site-exchange processes, indicating that the dynamics are not dictated by static energetic potentials. Instead, the activation energies for rotations in the crystals of **2** are controlled by temperature dependent local structural fluctuations and crystal fluidity.

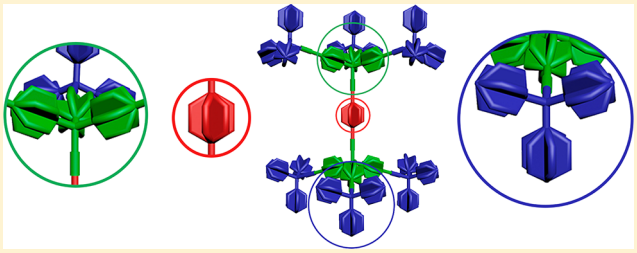

INTRODUCTION

While exploring the design of structures capable of supporting the functions of molecular machines,[1,2] our group has proposed the use of *amphidynamic crystals* featuring molecular gyroscopes and other molecular rotors with static frames and dynamic components.[3−5] Compound **1** is one of the simplest molecular gyroscopes with an open topology that we have analyzed in some detail[5f,g] (Figure 1). It consists of a phenylene rotator at the center linked by a double alkyne axle to a stator comprised of two triphenylmethyl (trityl) groups. The dumbbell shape of **1** makes it difficult for it to pack efficiently and generates a low-density region in the middle of the structure that, along with local volume fluctuations,[4e] allows for rotation of the central phenylene. Using variable temperature (VT) solid-state quadrupolar echo ^{2}H NMR spectroscopy (SS ^{2}H NMR), cross-polarization magic angle spinning (CPMAS) ^{13}C NMR spectroscopy, and computational analysis, we showed that the trityl stators engaged in a relatively tight 6-fold edge-to-face phenyl embrace are static, while the central rotator experiences a thermally activated 180° site exchange with a frequency of ca. 15 kHz at 297 K.[5f] More recently, we and others have described new examples of amphidynamic crystals with a range of internal dynamics.[4,6] Some of them have promising applications as novel materials with dielectric[4f,6a,d] and ferroelectric[6g,i,j] functions.

Considering strategies to increase the size of molecular gyroscopes to the range of biomolecular machines,[7] we decided to explore strategies to expand the architecture of **1** in a self-similar, radially growing manner. We viewed compound **2** as a promising target to obtain a well-ordered amphidynamic crystal based on its highly symmetric, shape-persistent, hyperbranched structure, and its many shape-conserving conformational degrees of freedom. We report here the synthesis, structure, and dynamic processes in **2**, a unique type of amphidynamic crystal. Crystals of this high molecular weight organic substance were obtained only from unconventional solvent mixtures. The crystal structure of **2** confirms the formation of a low-density crystal with a large amount of solvent molecules and intermolecular contacts reminiscent of a protein crystal. A close look at the structure suggested that motion might not be restricted to the central phenylene rotator (shown in red in Figure 1) but might extend to the phenylene branches (shown in green) and into the peripheral phenyl groups (shown in blue). With that in mind and taking advantage of a very efficient

Received: February 6, 2016
Published: March 14, 2016

DOI: 10.1021/jacs.6b01398
J. Am. Chem. Soc. 2016, 138, 4650−4656

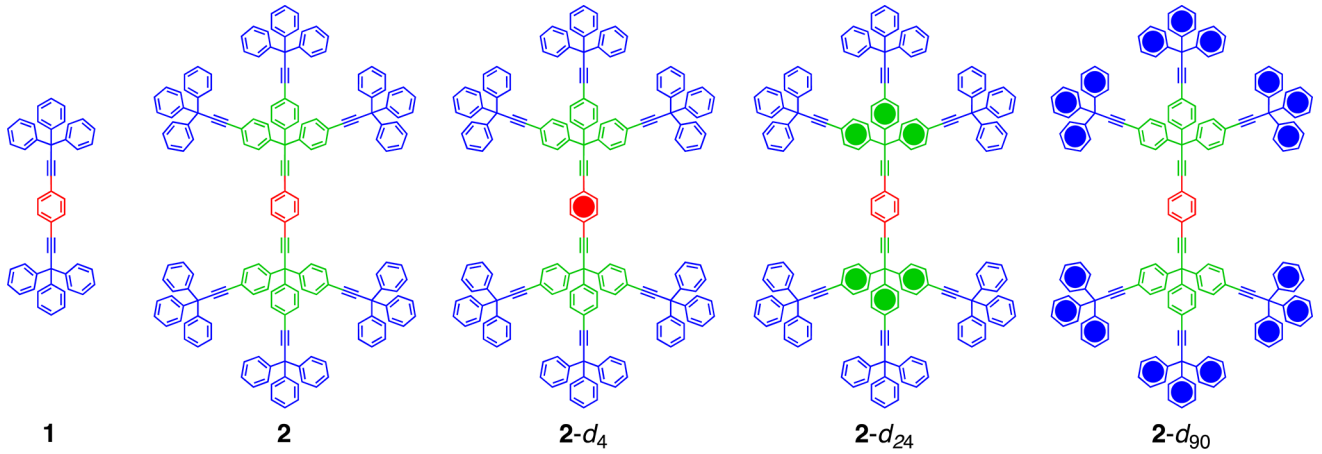

Figure 1. Structures of molecular rotor **1**, dendrimeric molecular rotor **2**, and its isotopologues **2**-d_4, **2**-d_{24}, and **2**-d_{90} with the filled circles indicating perdeuterated phenylene and phenyl groups.

modular synthesis, we prepared deuterated isotopologues **2**-d_4, **2**-d_{24}, and **2**-d_{90} to analyze their rotational dynamics. SS ^{2}H NMR measurements described here reveal ambient temperature rotational motion in the megahertz regime, indicating a crystal structure where every aromatic group displays fast rotational dynamics, whether it is the central phenylene rotator, phenylene groups in the trityl branches, or phenyl groups in the peripheral trityl groups. Crystals of dendritic rotor **2** represent a new type of amphidynamic crystals in which the frame of reference is solely determined by the C−C single bond framework and the quaternary carbons, which retain their equilibrium positions in the lattice while everything else rotates. Rotational dynamics as a function of temperature indicate that this unusually mobile environment is characterized by relatively high activation energies ($E_a \approx 15$ kcal/mol) and very large pre-exponential factors ($A \approx 10^{18}$ s^{-1}). In a structure where every aromatic group undergoes thermally activated rotations, an unusually large pre-exponential factor suggests that those dynamic processes are influenced by changes in the internal fluidity of the crystal lattice, rather than a static potential energy hypersurface of a simple site-exchange process.

RESULTS AND DISCUSSION

Synthesis and Characterization. Dendrimeric molecular rotor **2** was synthesized by taking advantage of the convergent strategy illustrated in Scheme 1. Sonagashira reaction between 3,3,3-triphenylpropyne **3**[5g] and 4-bromo-iodobenzene occurred selectively at the iodine site to give aryl bromide **4**. Treatment of **4** with *n*-butyllithium provided an aryllithium species, which was trapped with diethyl carbonate to give triarylmethanol **5**. When refluxed in a mixture of acetyl chloride and toluene, triarylmethanol **5** was converted to a triarylmethyl chloride intermediate, which was further reacted with ethynyl magnesium bromide to yield triarylpropyne **6**. Although palladium catalyzed coupling reactions of two large components are generally difficult,[8] we were able to achieve a double Sonagashira coupling reaction between terminal alkyne **6** and 1,4-diiodobenzene. Under optimized reaction conditions, rotor **2** could be obtained in 70% isolated yield and the homocoupling side reaction of **6** (not shown) was suppressed.

Isotopologues **2**-d_4, **2**-d_{24}, and **2**-d_{90} were prepared employing similar reactions with deuterated starting materials, 1,4-dibromobenzene-d_4 and **3**-d_{15},[9] to establish the desired isotopic labels. For details of the synthesis, please see the Supporting Information. Rotors **2**, **2**-d_4, **2**-d_{24}, and **2**-d_{90} were all fully characterized by solution ^{1}H and ^{13}C NMR, IR, and MALDI-TOF MS. Splitting of corresponding carbon signals could be observed in the ^{13}C NMR for rotors **2**-d_4, **2**-d_{24}, and **2**-d_{90} due to the C−D couplings (J = 22−25 Hz). The intensities of C−H stretching peaks (3000−3100 cm^{-1}) and C−H out-of-plane bending peaks (650−850 cm^{-1}) in IR of isotopologues **2**-d_{24} and **2**-d_{90} were significantly reduced resulting from the deuterium substitutions. To our surprise, the retention value (R_f) of isotopologue **2**-d_{90} (0.47) on a thin-layer chromatography (TLC) plate is different from those of rotors **2**, **2**-d_4, and **2**-d_{24} (0.49). This is a rather rare example of TLC separation of isotopologues,[10] and it could be explained by a reduced hydrodynamic radius of the molecule due to the collective effects of polydeuteration at the periphery.[11]

Scheme 1[a]

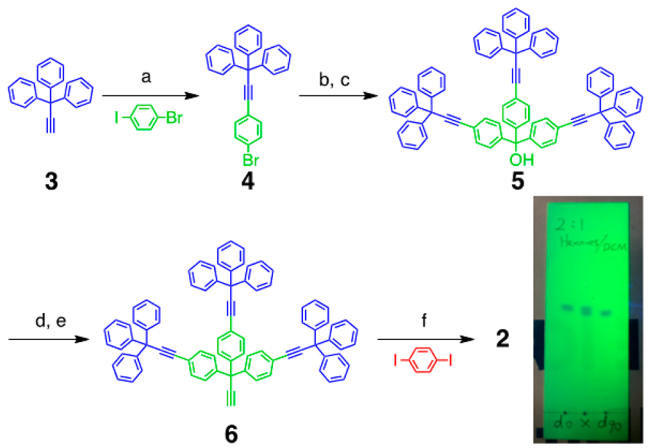

[a]Reagents and conditions: (a) $PdCl_2(PPh_3)_2$, CuI, THF, *i*-Pr_2NH, reflux, 91%; (b) *n*-BuLi, THF; then (c) diethyl carbonate, −78 °C to rt, 85%; (d) AcCl, Tol, reflux; (e) THF, ethynylmagnesium bromide, Tol, reflux, 63% over 2 steps; (f) $Pd(PPh_3)_4$, CuI, NEt_3, PPh_3, DMF, 70 °C, 70%. TLC plate illustrating the separation of **2** and **2**-d_{90} in the middle lane.

Crystallization and X-ray Structure of Dendrimeric Molecular Rotor 2. Crystallization of large organic molecules has always been a daunting challenge. To date, there are only a handful of crystal structures of compounds with molecular weight over 2000 Da reported in literature.[8b,12] Fortunately, we

DOI: 10.1021/jacs.6b01398
J. Am. Chem. Soc. 2016, 138, 4650−4656

obtained good quality crystals from warm supersaturated solutions of **2** and its isotopologues in a nonconventional solvent mixture containing 2,4,6-trimethylpyridine and 2,2,4-trimethylpentane.[13] X-ray diffraction data was collected at 100 K, and the crystal structure was solved in the triclinic space group $P\bar{1}$. The asymmetric unit consists of one-half of the rotor molecule together with about four solvent molecules, most of them being 2,4,6-trimethylpyridine. Since some of the solvent molecules are highly disordered and could not be modeled accurately, they were removed using the SQUEEZE algorithm.[14] As shown in Figure 2, the three C−Ph bond vectors of

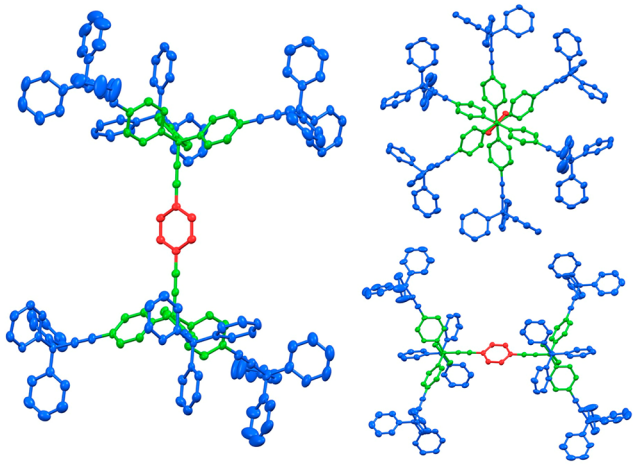

Figure 2. (left) Crystal structure of dendritic rotor **2** with thermal ellipsoids showing 50% probability. Solvent molecules and hydrogen atoms are omitted for clarity. (top right) View down the principal molecular axis and (bottom right) side view of **2** showing the *anti* conformations, respectively, between branch (green) trityls and the branch (green) and the peripheral (blue) trityls.

the inner trityl groups on the sides of the structure adopt *anti* conformations, as is commonly seen in crystals of molecular gyroscopes of this type.[5] A similar disposition can be observed for the peripheral trityls. Interestingly, all four trityl groups in the one-half of each rotor (Figure 2, left) have *P* or *PPP* helicity, while the other four related by an inversion center have *M* or *MMM* helicity. The inner alkyne axles display a slight deviation from linearity as measured by an angle of 175° measured from the *ipso* carbon of the central phenylene rotator to the center of the alkyne bond to the trityl quaternary carbon. Further analysis of the crystal structure shows the packing coefficient is only 0.46 without including the solvent molecules,[15] which is very low compared with the typical range (from 0.64 to 0.77) for organic molecules.[16] As a result, very few rotor−rotor close contacts were observed, mostly describable in terms of edge-to-face aromatic interactions. For example, the two faces of the central phenylene (C in Figure 3) are in close proximity to the edges of trityl branch phenylenes from two neighbors (B—C—B), and its two edges are directed toward the face of peripheral phenyl rings from neighboring molecules (P—C—P). Each of the branch phenylenes has only one close contact either with the central phenylene (B—C) or with one of the peripheral phenyl rings (not shown). The peripheral phenyl rings have less than two close contacts on average with other phenyl/phenylene rings. These observations support our hypothesis that the hyperbranched structure would lead to fewer interactions in the crystal, which is imperative to the realization of fast dynamics. It should be noted that while

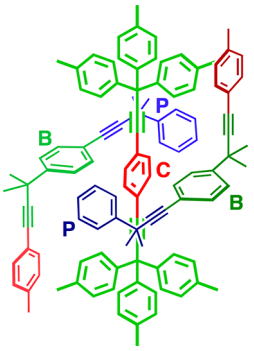

Figure 3. Schematic representation of the packing environment of the central phenylene (C) engaged in edge-to-face interactions acting as an acceptor with a branch phenylene (B) and as a donor with a peripheral (P) phenyl group.

solvent molecules are likely to be highly mobile, they also play an important role supporting the crystal structure, just like water molecules in protein crystals.[17] In fact, while attempting to obtain a crystal structure at 200 K, we noticed that all solvent molecules were disordered and none of them could be properly refined.

Variable Temperature Solid State ^{2}H NMR Experiments. ^{2}H NMR spectroscopy is a widely used technique to analyze the internal dynamics of deuterium-enriched groups in the 10^3−10^8 Hz regime in the solid state.[18] The method relies on static sample measurements acquired with the quadrupolar spin echo pulse sequence and is based on the changes in line shape that result from the dynamic narrowing of the broad powder pattern in the static spectra. Since the line shape is sensitive to both the trajectory and frequency of the site exchange dynamics, simulation of the experimental spectra usually provides sufficient information to characterize motions in solids in great detail.[19] The ^{2}H NMR spin−echo experiments were performed on crystalline and amorphous samples of **2**-d_4, **2**-d_{24}, and **2**-d_{90} to explore the dynamics of the central phenylene, branch phenylenes, and peripheral phenyls selectively.[20] Spectra with good signal-to-noise ratios could be obtained for all the crystalline samples and the amorphous samples of **2**-d_{24} and **2**-d_{90}. To our satisfaction, spectra obtained for all crystalline samples of **2**-d_4, **2**-d_{24}, and **2**-d_{90} indicated the presence of fast dynamic processes of the corresponding moieties that could be slowed (to a few kilohertz) when the samples were cooled (Figure 4). Those components were mostly static in amorphous samples, but they could be rendered mobile with sufficient thermal energy.

The sharp peak at the center of the spectrum of the crystalline samples of **2**-d_4 is the isotropic peak resulting from a small fraction of **2**-d_4 dissolved in residual solvent. The line shape of rest of the spectra could be simulated with a model that considers a 2-fold flip for the phenylene group. The best simulation at 293 K suggested a rotational frequency of 7.0 MHz. Rotational frequencies estimated in a similar manner for spectra measured at 283, 273, 263, 253, and 243 K indicated closest matches at 3.2 MHz, 1.6 MHz, 400 kHz, 180 kHz, and 25 kHz, respectively. The spectra obtained for the amorphous sample of **2**-d_4 turned out to be very noisy, even after over 48 h of acquisition time, due to the combined effects of the low deuterium content (only four deuterium atoms in one molecule) and the lower sensitivity of SS ^{2}H NMR in amorphous samples. Next we examined the ^{2}H NMR spectra of **2**-d_{24} at various temperatures. The spectra obtained for the

DOI: 10.1021/jacs.6b01398
J. Am. Chem. Soc. 2016, 138, 4650−4656

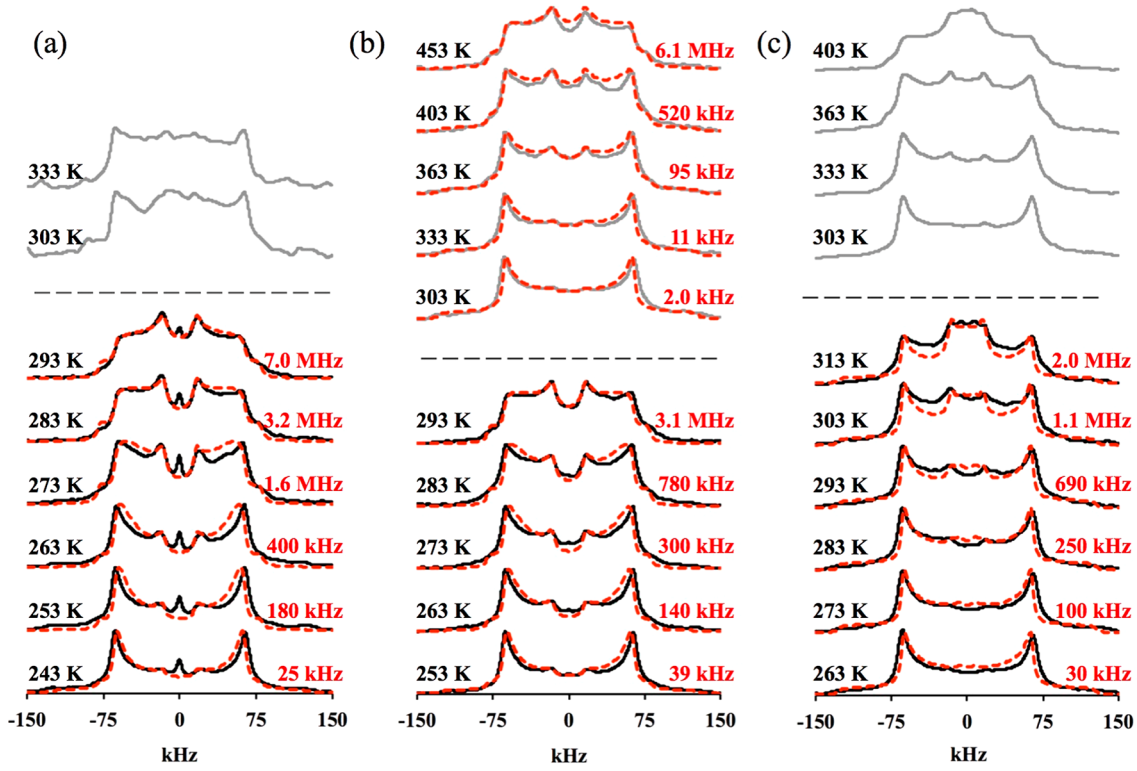

Figure 4. Experimental (black solid lines for the crystalline samples and gray solid lines for the amorphous samples) and simulated (red dashed lines) SS ^{2}H NMR spectra of (a) rotor **2**-d_4, (b) rotor **2**-d_{24}, and (c) rotor **2**-d_{90} at variable temperatures.

crystalline sample could be simulated well by considering a 2-fold-flip model with a log-Gaussian distribution[18,21] of the rotational frequencies having a width σ = 0.5. Rates of rotation at 293, 283, 273, 263, and 253 K were estimated to be 3.1 MHz, 780 kHz, 300 kHz, 140 kHz, and 39 kHz, respectively. The need for a Gaussian distribution may be attributed to the coexistence of three crystallographically nonequivalent branch phenylenes in the sample. The ^{2}H NMR spectra for amorphous sample of **2**-d_{24} measured at 303 K showed a static powder pattern, indicating that motions in a glassy state are slower. As the amorphous sample was heated, line shape changes were also consistent with a 2-fold flipping process, just like the crystalline sample, but with a larger distribution of exchange rates (σ = 2). Rotational exchange frequencies for experimental spectra measured at 453, 403, 363, 333, and 303 K corresponded to 6.1 MHz, 520 kHz, 95 kHz, 11 kHz, and 2.0 kHz.

The ^{2}H NMR spectra of the peripheral phenyl groups measured with samples of **2**-d_{90} are characterized by a rather complex superposition of a static signal, corresponding to the deuterium atom at the *para*-position, plus the signal of the other four deuterium atoms that are *ortho* and *meta* to the point of attachment of the phenyl ring. Since the C−D bond vector of the *para*-deuterium is aligned with the rotational axis (C−Ph bonds), its orientation does not change with rotation and its signal remains constant. By contrast, the other four C−D bonds have a cone angle of ±60° with respect to the rotational axis, such that any angular displacement can cause changes in the line shape of the spectrum. As shown in the right column in Figure 4, the spectral data of **2**-d_{90} started with a spectrum approaching the slow exchange regime at 263 K and displayed spectral changes characteristic of increasing motion as the sample temperature reached 313 K. Notably, a simple 180° site exchange model could not provide a reasonable simulation for the experimental spectra (Figure S45). Instead, the experimental data could be reproduced reasonably well with a 4-fold rotation model and a 2:1 population distribution (Figure S46) on nonequivalent sites related by 90°. This model led to site exchange rates of 2.0 MHz, 1.1 MHz, 690 kHz, 250 kHz, 100 kHz, and 30 kHz at 313, 303, 293, 283, 273, and 263 K, respectively.

This model is an approximation because the real system has nine noncrystallographically equivalent peripheral phenyl groups, each with a potentially different site exchange rate. It is not surprising that the same 4-fold rotation model with a 2:1 population could only provide a qualitative simulation for the spectra of the amorphous **2**-d_{90} samples with all phenyl groups rotating independently. This also suggests that rotational trajectories are dictated by molecular structures while rotational frequencies and their temperature dependence are determined by the crystallinity of the samples.

While it would be insightful to document the dynamics of the solvent, we were not able to observe them directly using NMR spectroscopy. Because the crystals are fragile and tend to lose solvent, all measurements had to be carried out in the presence of excess of solvent supernatant. As a result, the signals corresponding to solvent molecules in the crystal lattice could not be identified.

Mechanisms of Rotation of Branch Phenylene and Peripheral Phenyl Groups: Correlated Trityl Group Rotations. While the rotational dynamics of the central phenylene in **2**-d_4 are well accounted for by a 2-fold site exchange involving 180° rotations between degenerate sites, the branch phenylenes in **2**-d_{24} and the peripheral phenyl groups in **2**-d_{90} are part of trityl groups and could be expected to undergo correlated (gearing) motions. The fact that suitable simulations for **2**-d_{24} required only a 2-fold site exchange model while those

DOI: 10.1021/jacs.6b01398
J. Am. Chem. Soc. 2016, 138, 4650−4656

for **2**-d_{90} required a 4-fold site exchange with unequal populations was investigated. We examined the rotational mechanisms for compound **2** with molecular dynamics (MD) simulations using the AMBER14 program.[22] The parameters were generated with the antechamber module using the general Amber force field (GAFF) and atomic partial charges were assigned using the AM1-BCC method (SI, p S63). Activation free energies in vacuum were obtained for different rotational mechanisms using umbrella sampling, and potentials of mean force (PMF) were constructed using the weighted histogram analysis method (WHAM), with the dihedral angles extracted every 50 fs.[23] As suggested by the space-filling model (Figure 5a), a 2-fold rotation of one phenylene while the other two are

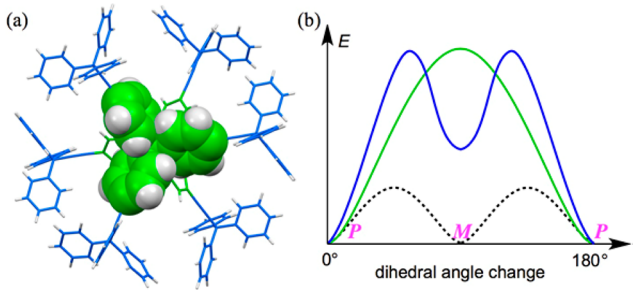

Figure 5. (a) Space filling representation of a branch phenylene trityl group indicating the necessity of a correlated process to allow for 2-fold 180° rotations. (b) Energy changes of correlated phenylene rotation in a trityl group in vacuum corresponding for apparent 2-fold (green solid curve) and 4-fold (blue solid curve and black dashed curve) rotation modes.

completely static is an energetically demanding process because of the proximity of the three phenylene groups. With a calculated barrier of ca. 19 kcal/mol in the vacuum, it is unlikely to occur in the solid state. However, it is possible to have independent rotation of one ring while the other two are oscillating, and the corresponding activation energy was estimated to be only 3−5 kcal/mol in vacuum. Alternatively, the three rings could rotate synchronously to change the absolute configuration of the chiral propeller conformation of the trityl group, a process extensively studied by Mislow and others.[24] In vacuum, this enantiomerization process is associated with angular displacements of ca. 90° and energy barriers of about 1 kcal/mol (Figure 5b, dashed curves). Analysis of the lowest energy trajectory suggests a "2-ring flip" mechanism, as proposed by Mislow for trityl isomerization in solution. In the crystal, however, the two enantiomers (*P* and *M*) are in a chiral environment and have different energies. Consequently, if one enantiomer is much higher in energy in the crystal (Figure 5b, blue curve), an effective 2-fold rotation (from one *P*-enantiomer to a transient *M* enantiomer to the next *P*-enantiomer) would be observed, instead of a 4-fold rotation. Under the most extreme circumstances, one enantiomer could be a local maximum (transition state of rotation) and the correlated motion of three phenylenes would also appear to be 2-fold rotations (Figure 5b, green curve). As a result, while the experimental data and MD simulation are both consistent with an effective 2-fold rotation in the case of **2**-d_{24}, it is not possible to distinguish between correlated motion of three phenylenes and the independent rotation of one phenylene while the other two oscillate.

The mechanisms of rotation for the peripheral phenyl groups in **2**-d_{90} samples can be analyzed also as discussed above and considering the potentials shown in Figure 5b. In fact, the experimentally observed 4-fold rotational model can be understood in terms of a trityl enantiomerization process where the crystallographically observed enantiomer is lower in energy but the second enantiomer is thermally accessible. Thus, a ca. 2:1 population distribution suggested that the two enantiomers (*P* and *M*) are both local minima and the energy difference between them is small (Figure 5b, blue curve). This is also consistent with the crystal structure, where the periphery phenyls displayed larger thermal ellipsoids than the rest of the rotor structure.

Activation Parameters. The Arrhenius plots constructed from the rotational exchange frequencies observed at each of the experimental temperatures for the central phenylene (**2**-d_4), branch phenylenes (**2**-d_{24}), and peripheral phenyls (**2**-d_{90}) are shown in Figure 6. The most significant result is that all the

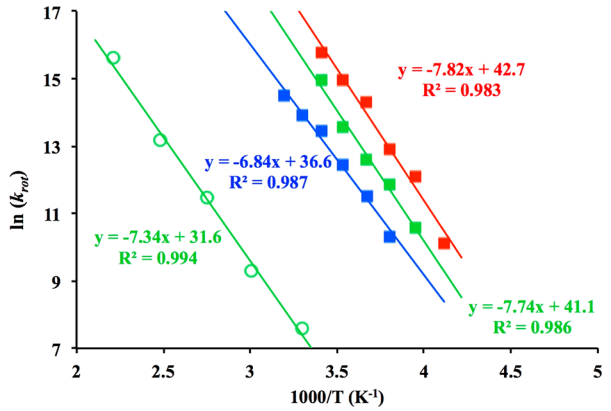

Figure 6. Arrhenius plots for crystalline (filled squares) and amorphous samples (open circles) of **2**-d_4 (red), **2**-d_{24} (green), and **2**-d_{90} (blue).

aromatic groups of the rotor in the crystals undergo rapid site exchange dynamics near ambient temperature. For the crystalline samples (Table 1), the corresponding activation

Table 1. Summary of Apparent[a] Activation Parameters

sample	E_a (kcal/mol)	A (s^{-1})
2-d_4, crystalline	15.7	3.5×10^{18}
2-d_{24}, crystalline	15.5	7.8×10^{17}
2-d_{24}, amorphous	14.7	5.3×10^{13}
2-d_{90}, crystalline	13.7	7.8×10^{15}

[a]Please see discussion in main text.

energies (E_a) and pre-exponential factors (A) are 15.7 kcal/mol and 3.5×10^{18} s^{-1} for **2**-d_4, 15.5 kcal/mol and 7.8×10^{17} s^{-1} for **2**-d_{24}, and 13.7 kcal/mol and 7.8×10^{15} s^{-1} for **2**-d_{90}. Similar activation parameters obtained for different aromatic segments in the molecule are consistent with the fact that all of them share contacts and thus have a shared potential (Figure 3).

It is important to note that pre-exponential factors on the order of 10^{16}−10^{18} s^{-1} cannot be associated with an elementary process, such as the torsional mode that becomes an internal rotation when provided with sufficient thermal energy. In fact, elementary rotations involving phenylene groups are limited to values on the order of ca. 10^{12} s^{-1}, as shown by quantum mechanical calculations of the corresponding torsional mode or by classical mechanics calculations based on its moment of inertia.[25] Numerous previous studies with crystalline phenylene

DOI: 10.1021/jacs.6b01398
J. Am. Chem. Soc. 2016, 138, 4650−4656

rotors have also revealed pre-exponential values of this magnitude, with exceptions encountered when noncrystalline samples are analyzed.[26] We have previously suggested that abnormally high pre-exponential factors in the solid state can be associated with changes in the fluidity of the structure, rather than with a static potential of the corresponding motions. For example, when exploring the temperature dependence of the rotational dynamics of a *p*-phenylene group in a periodic mesoporous organosilicate (PMO), we obtained nonlinear data within a temperature region indicating an apparent activation energy of 47 kcal/mol and an apparent pre-exponential value of 4.0×10^{41} s^{-1}, both of which are, of course, nonsensical.[26] Further analysis based on differential scanning calorimetry (DSC) supported a reasonable interpretation for the observed results. It was shown that the steep slope of the rotational frequency vs inverse temperature in the corresponding Arrhenius plot was the result of the structural softening that occurs when the 2D rigid glass becomes a 2D rotational fluid, during a second order glass transition. In a similar manner, we propose that a large slope and intercept in the Arrhenius plot of crystalline dendrimeric molecular rotor **2** is the result of a crystal structure that becomes increasingly soft, or more "fluid-like", as the temperature increases. We suggest the term *crystal fluidity* to convey the softening of the local environment in crystals that results from the temperature-dependent conformational motions, librations, group rotations, and presumably solvent dynamics.

If we assume that the correct pre-exponential factor for any given potential is dictated by the torsional motion of a phenylene with a constant value of ca. 1.0×10^{12} s^{-1}, we can estimate a "corrected" activation energy for every temperature. In the case of **2**-d_4, the experimental data would be consistent with an energy barrier that changes from 7.9 kcal/mol at 253 K, when the structure is relatively rigid, to a barrier of 6.9 kcal/mol at 293 K as the structure becomes more fluid. A similar analysis for the data obtained in the case of **2**-d_{24} gives what would be "corrected" activation energies of 8.6 and 7.4 kcal/mol at 253 and 293 K, respectively. Thus, it is reasonable to conclude that the dynamic behavior observed with crystals of **2**-d_4 and **2**-d_{24} is the result of a barrier change of ca. 1 kcal/mol over a rather modest temperature range of only 40 K. A similar analysis with samples of amorphous **2**-d_{24} showed that variations in the "corrected" activation energy over a similar temperature interval are much smaller (Table S1). Furthermore, an interpretation based on a decreasing barrier is also consistent with the fact that all aromatic groups are undergoing temperature-activated, fast rotational dynamics, such that their local potential becomes increasingly fluid.

CONCLUSIONS

A highly efficient convergent strategy was developed for the synthesis of a macromolecular dendritic rotor in its natural abundance and selectively deuterated forms to carry out quadrupolar echo ^{2}H NMR line shape analysis. Amphidynamic crystals obtained from a mixture of 2,4,6-trimethylpyridine and 2,2,4-trimethylpentane showed a low-density structure that allows for the fast rotation of all the aromatic groups, including one located at the core, six at the branches, and 18 at the periphery. It is notable that the rotational frequencies of the three segments of the structures reach the megahertz regime near ambient temperatures and exhibit similar activation parameters. While close activation energies are consistent with rotational potentials based on interactions between the three parts of the structure, pre-exponential factors that are up to 6 orders of magnitude larger than those expected for elementary processes are interpreted in terms of a temperature-induced softening of the packing structure. These observations indicate that rotational dynamics in this hyperbranched structure depend more on the fluidity of the crystal than on the contacts and interactions that would make up a static potential derived from the equilibrium position of the atoms in the structure.

ASSOCIATED CONTENT

Supporting Information

The Supporting Information is available free of charge on the ACS Publications website at DOI: 10.1021/jacs.6b01398.

Synthesis and spectroscopic characterization of dendrimeric rotor **2** and its isotopologues, solid-state NMR simulations, and details of the molecular dynamics simulations (PDF)

Crystallographic data for **2** (CIF)

AUTHOR INFORMATION

Corresponding Authors

*houk@chem.ucla.edu

*mgg@chem.ucla.edu

Notes

The authors declare no competing financial interest.

ACKNOWLEDGMENTS

We thank Dr. Jane Strouse and Dr. Robert Taylor for assistance with NMR measurements and Dr. Gonzalo Jiménez-Osés for helpful discussions. This work was supported by the National Science Foundation through Grants DMR1101934 and DMR140268 (M.A.G.-G.) and CHE1361104 (K.N.H.).

REFERENCES

(1) (a) Abendroth, J. M.; Bushuyev, O. S.; Weiss, P. S.; Barrett, C. J. *ACS Nano* **2015**, *9*, 7746. (b) Erbas-Cakmak, S.; Leigh, D. A.; McTernan, C. T.; Nussbaumer, A. L. *Chem. Rev.* **2015**, *115*, 10081. (c) Coskun, A.; Banaszak, M.; Astumian, R. D.; Stoddart, J. F.; Grzybowski, B. A. *Chem. Soc. Rev.* **2012**, *41*, 19. (d) Kinbara, K.; Aida, T. *Chem. Rev.* **2005**, *105*, 1377. (e) Kottas, G. S.; Clarke, L. I.; Horinek, D.; Michl, J. *Chem. Rev.* **2005**, *105*, 1281.

(2) (a) Cheng, C.; McGonigal, P. R.; Schneebeli, S. T.; Li, H.; Vermeulen, N. A.; Ke, C.; Stoddart, J. F. *Nat. Nanotechnol.* **2015**, *10*, 547. (b) Li, Q.; Fuks, G.; Moulin, E.; Maaloum, M.; Rawiso, M.; Kulic, I.; Foy, J. T.; Giuseppone, N. *Nat. Nanotechnol.* **2015**, *10*, 161. (c) Ragazzon, G.; Baroncini, M.; Silvi, S.; Venturi, M.; Credi, A. *Nat. Nanotechnol.* **2015**, *10*, 70. (d) De, S.; Pramanik, S.; Schmittel, M. *Angew. Chem., Int. Ed.* **2014**, *53*, 14255. (e) Conyard, J.; Cnossen, A.; Browne, W. R.; Feringa, B. L.; Meech, S. R. *J. Am. Chem. Soc.* **2014**, *136*, 9692. (f) Lewandowski, B.; De Bo, G.; Ward, J. W.; Papmeyer, M.; Kuschel, S.; Aldegunde, M. J.; Gramlich, P. M. E.; Heckmann, D.; Goldup, S. M.; D'Souza, D. M.; Fernandes, A. E.; Leigh, D. A. *Science* **2013**, *339*, 189. (g) Perera, U. G. E.; Ample, F.; Kersell, H.; Zhang, Y.; Vives, G.; Echeverria, J.; Grisolia, M.; Rapenne, G.; Joachim, C.; Hla, S.-W. *Nat. Nanotechnol.* **2013**, *8*, 46. (h) Thies, S.; Sell, H.; Schütt, C.; Bornholdt, C.; Näther, C.; Tuczek, F.; Herges, R. *J. Am. Chem. Soc.* **2011**, *133*, 16243. (i) Hess, G. D.; Hampel, F.; Gladysz, J. A. *Organometallics* **2007**, *26*, 5129.

(3) (a) Vogelsberg, C. S.; Garcia-Garibay, M. A. *Chem. Soc. Rev.* **2012**, *41*, 1892. (b) Khuong, T.-A. V.; Nuñez, J. E.; Godinez, C. E.; Garcia-Garibay, M. A. *Acc. Chem. Res.* **2006**, *39*, 413. (c) Garcia-Garibay, M. A. *Proc. Natl. Acad. Sci. U. S. A.* **2005**, *102*, 10771.

DOI: 10.1021/jacs.6b01398
J. Am. Chem. Soc. 2016, 138, 4650−4656

(4) (a) Pérez-Estrada, S.; Rodríguez-Molina, B.; Xiao, L.; Santillan, R.; Jiménez-Osés, G.; Houk, K. N.; Garcia-Garibay, M. A. *J. Am. Chem. Soc.* **2015**, *137*, 2175. (b) Jiang, X.; Rodríguez-Molina, B.; Nazarian, N.; Garcia-Garibay, M. A. *J. Am. Chem. Soc.* **2014**, *136*, 8871. (c) Commins, P.; Garcia-Garibay, M. A. *J. Org. Chem.* **2014**, *79*, 1611. (d) Rodríguez-Molina, B.; Farfán, N.; Romero, M.; Méndez-Stivalet, M. J.; Santillan, R.; Garcia-Garibay, M. A. *J. Am. Chem. Soc.* **2011**, *133*, 7280. (e) Jarowski, P. D.; Houk, K. N.; Garcia-Garibay, M. A. *J. Am. Chem. Soc.* **2007**, *129*, 3110. (f) Horansky, R. D.; Clarke, L. I.; Price, J. C.; Khuong, T.; Jarowski, P. D.; Garcia-Garibay, M. A. *Phys. Rev. B: Condens. Matter Mater. Phys.* **2005**, *72*, 014302.

(5) (a) O'Brien, Z. J.; Natarajan, A.; Khan, S.; Garcia-Garibay, M. A. *Cryst. Growth Des.* **2011**, *11*, 2654. (b) Karlen, S. D.; Reyes, H.; Taylor, R. E.; Khan, S. I.; Hawthorne, M. F.; Garcia-Garibay, M. A. *Proc. Natl. Acad. Sci. U. S. A.* **2010**, *107*, 14973. (c) Rodríguez-Molina, B.; Ochoa, M. E.; Farfán, N.; Santillan, R.; Garcia-Garibay, M. A. *J. Org. Chem.* **2009**, *74*, 8554. (d) Khuong, T.-A. V.; Dang, H.; Jarowski, P. D.; Maverick, E. F.; Garcia-Garibay, M. A. *J. Am. Chem. Soc.* **2007**, *129*, 839. (e) Dominguez, Z.; Khuong, T.; Dang, H.; Sanrame, C. N.; Nuñez, J. E.; Garcia-Garibay, M. A. *J. Am. Chem. Soc.* **2003**, *125*, 8827. (f) Dominguez, Z.; Dang, H.; Strouse, M. J.; Garcia-Garibay, M. A. *J. Am. Chem. Soc.* **2002**, *124*, 7719. (g) Dominguez, Z.; Dang, H.; Strouse, M. J.; Garcia-Garibay, M. A. *J. Am. Chem. Soc.* **2002**, *124*, 2398.

(6) (a) Harada, J.; Ohtani, M.; Takahashi, Y.; Inabe, T. *J. Am. Chem. Soc.* **2015**, *137*, 4477. (b) Zhu, K.; O'Keefe, C. A.; Vukotic, V. N.; Schurko, R. W.; Loeb, S. J. *Nat. Chem.* **2015**, *7*, 514. (c) Comotti, A.; Bracco, S.; Yamamoto, A.; Beretta, M.; Hirukawa, T.; Tohnai, N.; Miyata, M.; Sozzani, P. *J. Am. Chem. Soc.* **2014**, *136*, 618. (d) Zhang, Q.-C.; Wu, F.-T.; Hao, H.-M.; Xu, H.; Zhao, H.-X.; Long, L.-S.; Huang, R.-B.; Zheng, L.-S. *Angew. Chem., Int. Ed.* **2013**, *52*, 12602. (e) Setaka, W.; Yamaguchi, K. *J. Am. Chem. Soc.* **2013**, *135*, 14560. (f) Lemouchi, C.; Iliopoulos, K.; Zorina, L.; Simonov, S.; Wzietek, P.; Cauchy, T.; Rodríguez-Fortea, A.; Canadell, E.; Kaleta, J.; Michl, J.; Gindre, D.; Chrysos, M.; Batail, P. *J. Am. Chem. Soc.* **2013**, *135*, 9366. (g) Zhang, Y.; Zhang, W.; Li, S.-H.; Ye, Q.; Cai, H.-L.; Deng, F.; Xiong, R.-G.; Huang, S. D. *J. Am. Chem. Soc.* **2012**, *134*, 11044. (h) Vukotic, V. N.; Harris, K. J.; Zhu, K.; Schurko, R. W.; Loeb, S. J. *Nat. Chem.* **2012**, *4*, 456. (i) Akutagawa, T.; Koshinaka, H.; Sato, D.; Takeda, S.; Noro, S.-I.; Takahashi, H.; Kumai, R.; Tokura, Y.; Nakamura, T. *Nat. Mater.* **2009**, *8*, 342. (j) Jain, P.; Dalal, N. S.; Toby, B. H.; Kroto, H. W.; Cheetham, A. K. *J. Am. Chem. Soc.* **2008**, *130*, 10450.

(7) (a) Schliwa, M.; Woehlke, G. *Nature* **2003**, *422*, 759. (b) Piccolino, M. *Nat. Rev. Mol. Cell Biol.* **2000**, *1*, 149.

(8) (a) May, R.; Jester, S.-S.; Höger, S. *J. Am. Chem. Soc.* **2014**, *136*, 16732. (b) Shen, X.; Ho, D. M.; Pascal, R. A. *J. Am. Chem. Soc.* **2004**, *126*, 5798.

(9) Karlen, S. D.; Garcia-Garibay, M. A. *Chem. Commun.* **2005**, 189.

(10) Heck, H. D. A.; Simon, R. L.; Anbar, M. *J. Chromatogr.* **1977**, *133*, 281.

(11) Tanaka, N.; Thornton, E. R. *J. Am. Chem. Soc.* **1976**, *98*, 1617.

(12) (a) Kondratuk, D. V.; Sprafke, J. K.; O'Sullivan, M. C.; Perdigao, L. M. A.; Saywell, A.; Malfois, M.; O'Shea, J. N.; Beton, P. H.; Thompson, A. L.; Anderson, H. L. *Chem. - Eur. J.* **2014**, *20*, 12826. (b) Bauer, R. E.; Enkelmann, V.; Wiesler, U. M.; Berresheim, A. J.; Müllen, K. *Chem. - Eur. J.* **2002**, *8*, 3858. (c) Nielsen, M. B.; Schreiber, M.; Baek, Y. G.; Seiler, P.; Lecomte, S.; Boudon, C.; Tykwinski, R. R.; Gisselbrecht, J.-P.; Gramlich, V.; Skinner, P. J.; Bosshard, C.; Günter, P.; Gross, M.; Diederich, F. *Chem. - Eur. J.* **2001**, *7*, 3263. (d) Ipaktschi, J.; Hosseinzadeh, R.; Schlaf, P.; Dreiseidler, E.; Goddard, R. *Helv. Chim. Acta* **1998**, *81*, 1821.

(13) Crystals of almost identical cell parameters could be obtained from an *o*-xylene/2,2,4-trimethylpentane mixture with the only differences being the solvent molecules included in the crystals.

(14) Spek, A. *Acta Crystallogr., Sect. D: Biol. Crystallogr.* **2009**, *65*, 148.

(15) The packing coefficient increases to 0.69 when the solvent molecules in the crystal are included. Molecular volumes were calculated using the group increment approach reported in (a) Gavezzotti, A. *J. Am. Chem. Soc.* **1983**, *105*, 5220. (b) Bondi, A. *J. Phys. Chem.* **1964**, *68*, 441. The results agree closely with volumes calculated using (c) Spartan'08; Wavefunction, Inc.: Irvine, CA, 2008.

(16) Dunitz, J. D.; Gavezzotti, A. *Acc. Chem. Res.* **1999**, *32*, 677.

(17) (a) Schoenborn, B. P.; Garcia, A.; Knott, R. *Prog. Biophys. Mol. Biol.* **1995**, *64*, 105. (b) Richards, F. M. *Annu. Rev. Biophys. Bioeng.* **1977**, *6*, 151.

(18) Hansen, M. R.; Graf, R.; Spiess, H. W. *Acc. Chem. Res.* **2013**, *46*, 1996.

(19) Macho, V.; Brombacher, L.; Spiess, H. W. *Appl. Magn. Reson.* **2001**, *20*, 405.

(20) The SS ^{2}H NMR spectra for the crystalline samples were obtained in the presence of the solvent supernatant to avoid solvent loss and amorphization during the data acquisition. For all the VT experiments, samples were gradually heated or cooled from 293 K to the target temperature. Sample integrity and data reproducibility were analyzed by measuring the 293 K spectra at the end of each experiment.

(21) Structurally heterogeneous systems can often be described by a Gaussian distribution of activation energies, which gives rise to a log-Gaussian distribution of rates. Under these conditions, the weight $f(k)$ of a certain rate k is given by the following equation, where the most probable rate is k_0 and the width of the distribution is given by σ,

$$f(x) = \frac{1}{\sigma\sqrt{2\pi}}\, e^{(-x^2/(2\sigma^2))}$$

with $x = \ln(k/k_0)$.

(22) Case, D. A.; Babin, V.; Berryman, J.; Betz, R. M.; Cai, Q.; Cerutti, D. S.; Cheatham, T. E., III; Darden, T. A.; Duke, R. E.; Gohlke, H.; Goetz, A. W.; Gusarov, S.; Homeyer, N.; Janowski, P.; Kaus, J.; Kolossvary, I.; Kovalenko, A.; Lee, T. S.; LeGrand, S.; Luchko, T.; Luó, R.; Madej, B.; Merz, K. M.; Paesani, F.; Roe, D. R.; Roitberg, A.; Sagui, C.; Salomon-Ferrer, R.; Seabra, G.; Simmerling, C. L.; Smith, W.; Swails, J.; Walker, R. C.; Wang, J.; Wolf, R. M.; Wu, X.; Kollman, P. A. *AMBER 14*; University of California, San Francisco, 2014.

(23) Grossfield, A. Wham: the weighted histogram, analysis method, version 2.0.9, http://membrane.urmc.rochester.edu/content/wham, accessed Jan 27, 2016.

(24) Gust, D.; Mislow, K. *J. Am. Chem. Soc.* **1973**, *95*, 1535.

(25) Inertial rotational frequency, τ_{IR}^{-1}, can be estimated from the moment of inertia (I) of a rotator using the equation $\tau_{IR}^{-1} = [(2\pi/9)(I/[kBT])^{1/2}]^{-1}$, where I is moment of inertia measured along the rotational axis. Please see: Kawski, A. *Crit. Rev. Anal. Chem.* **1993**, *23*, 459.

(26) Vogelsberg, C. S.; Bracco, S.; Beretta, M.; Comotti, A.; Sozzani, P.; Garcia-Garibay, M. A. *J. Phys. Chem. B* **2012**, *116*, 1623.

DOI: 10.1021/jacs.6b01398
J. Am. Chem. Soc. 2016, 138, 4650−4656